Size Selectivity in Artificial Cilia–Particle Interactions: Mimicking the Behavior of Suspension Feeders

ARTICLE *in* LANGMUIR · MARCH 2013

Impact Factor: 4.46 · DOI: 10.1021/la400318f · Source: PubMed

3 AUTHORS, INCLUDING:

Amitabh Bhattacharya
University of Pittsburgh
41 PUBLICATIONS **147** CITATIONS

SEE PROFILE

Langmuir

Article

pubs.acs.org/Langmuir

Size Selectivity in Artificial Cilia–Particle Interactions: Mimicking the Behavior of Suspension Feeders

Anurag Tripathi,[†] Amitabh Bhattacharya,[‡] and Anna C. Balazs*,[†]

[†]Department of Chemical and Petroleum Engineering, 1249, Benedum Hall, University of Pittsburgh, Pittsburgh, Pennsylvania 15261, United States

[‡]Department of Mechanical Engineering, Indian Institute of Technology Bombay, Powai, Mumbai, 400076

ABSTRACT: Inspired by the ability of marine suspension feeders to selectively capture small particles by their hairlike cilia, we simulate the interaction between artificial cilia and microscopic particles of different sizes to determine if a purely synthetic system can display analogous size-selective behavior. Our computational approach specifically models the capture of particles suspended in the surrounding fluid by adhesive filaments, which are anchored by one end to a surface. Via this model, we show that this size selectivity can arise as a result of adhesive and hydrodynamic interactions in the system. The substantial reduction in the mobility of the large particles near surfaces leads to a failure in capturing large particles. Using a simple analytical model, we show that the balance of hydrodynamic and adhesive forces favors capture of particles below a critical size for a given cilia–particle interaction. Our findings provide guidelines for designing artificial cilia that can be used for sorting and transporting particles within microfluidic devices.

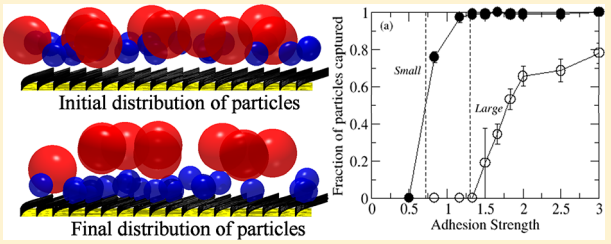

INTRODUCTION

Advances over the past decade have enabled the use of "artificial cilia" to perform vital functions in microfluidic devices, including the effective pumping and/or mixing of complex fluids within the microchambers.[1] The inspiration for such synthetic ciliary systems has come from biological organisms that harness cilia to perform a range of essential tasks. Marine suspension feeders provide a particularly inspiring example of the use of biological cilia. Namely, these marine organisms use hairlike cilia to collect food particles from ambient fluids, employing a process that involves three stages: particle encounter, capture of the suspended particle, and transportation to the mouth.[2−4] An adhesive interaction between the particle and cilia has long been proposed as a crucial step for capturing the encountered particles,[2,5,6] and recent studies[7] have provided conclusive evidence of the direct adhesion between the particles and cilia. A remarkable feature of such suspension feeders is their selective intake of particles below a particular size.[5−8] Size selection is observed predominately at the time of the initial particle pickup[5,6] and, hence, could be controlled by fundamental physical forces[6,9] operating as the particle and cilia come into contact. While morphological details of the ciliary systems vary across different suspension feeding species, a key minimum design occurs repeatedly: an array of beating cilia tethered to a surface (e.g., a tentacle or some other body part). Given the universal nature of this basic design and the fact that the particle pick up could be controlled by physiochemical interactions,[6,9] it is intriguing to consider if an artificial ciliated surface could display an analogous discrimination between particles of different sizes.

Herein, we use computational and analytical approaches to model systems that involve this minimum design concept and show that the size selectivity displayed by suspension feeders can arise simply as a result of competition between fundamental adhesive and hydrodynamic forces. Notably, there have been few modeling studies on cilia–particle interactions[10−13] despite the prevalence of such interactions in a broad range of vital biological phenomena, e.g., in the expulsion of particulates from the respiratory tract[14] and the transport of egg cells along the oviduct.[15,16] With the ever-increasing role of artificial cilia in microfluidics,[1,17] such studies are critical not only for obtaining basic insight into biological phenomena but also for designing new, high-performance devices with potential biomedical applications.[18,19]

In carrying out these studies, we extend our recently developed models for the interactions of ciliated surfaces with adhesive particles.[10] In the previous study,[10] we modeled the interaction of a single particle of a given size with the cilia layer; we did not consider the effect of particle size and the model did not encompass multiple particles. Furthermore, the analytical model did not account for the dependence of the particle mobility on size. In the computational model described below, we introduce multiple particles and account for the hydrodynamic interactions between these particles. We also modify the analytical model to determine the dependence of the drag force on particle size for particles near a surface. With these modifications, we can show that the competition between

Received: January 23, 2013
Revised: March 14, 2013

   dx.doi.org/10.1021/la400318f | *Langmuir* XXXX, XXX, XXX–XXX

adhesion and drag forces is sufficient to explain the size-selective intake of suspension feeders and, consequently, provide guidelines for designing ciliated surfaces that could be used for sorting particles based on their size as well as their adhesive properties.[10]

Below, we first describe our computational approach. In the ensuing section, we present the findings of these computational studies and describe the analytical calculations that we use to both validate the results from the simulations and obtain insight into the factors that give rise to the size-selective behavior of the ciliated substrate.

COMPUTATIONAL MODEL

Figure 1a shows a snapshot from our simulations. Our computer model encompasses a regular array of cilia that are

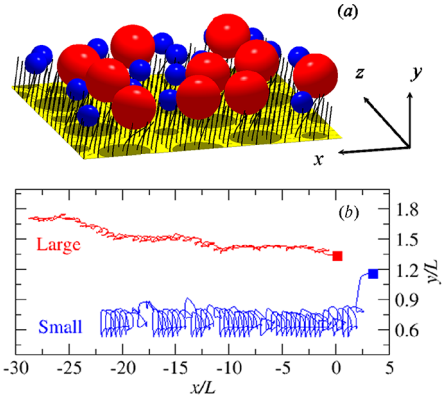

Figure 1. (a) A snapshot of the simulated system. Black filaments represent the cilia, and spheres are the particles of two different sizes. (b) Sample trajectories of a small and a large particle, beginning at filled squares, projected on the *xy* plane.

tethered to the bottom wall ($y = 0$) in a simulation box of size $L_x \times L_y \times L_z$, which is filled with a fluid of shear viscosity η. No slip boundary conditions are imposed at the $y = 0$ and $y = L_y$ walls, and periodic boundaries are applied in the *x*- and *z*-directions. The fluid velocity is evolved using the lattice Boltzmann method (LBM),[20] which is an efficient solver for the Navier–Stokes equation. Spherical particles of radii $R_S = 3$ LB units and $R_L = 6$ LB units are randomly dispersed within a layer that is approximately 3LB units thick in the *y*-direction and spans the area of the simulation box. In other words, particles are dispersed in the layer so that their minimum depth in the layer is 1 LB unit and maximum depth is 4 LB units. The position of the layer ensures that the minimum depth of the particles in the cilia layer is at least 1 LB unit, ensuring their interaction with the actuated cilia.

Each cilium is modeled as a chain of N beads (of radius a), connected by linear springs.[10] The elastic potential energy of the chain is given as $U = \sum_{i=1}^{N}(1/2)[k_s(|\mathbf{r}^i - \mathbf{r}^{i-1}| - l)^2 + k_b(\theta_i - \pi)^2]$, where θ_i is the angle between neighboring links, $\mathbf{r}^0$ is the tether point of the cilia, and k_s, k_b, and l are the respective stretching modulus, bending modulus, and the equilibrium distance between the beads. With $N = 9$ and $l = 1$ LB unit, the cilium length is $L = 9$ LB units; the intercilium spacing is $\delta_x = 4$ LB units.

The hydrodynamic coupling of a cilium bead with the fluid is captured using a frictional force that is proportional to the slip velocity between the bead and fluid.[10,21] The hydrodynamic interactions between the spherical particles and fluid are captured using bounce-back boundary conditions at the particle–fluid surface,[20] mimicking no slip boundary conditions at the particle surface.

To mimic the adhesive interaction between the particles and cilia, the top three beads of each cilium experience an attractive Morse-potential interaction with the particles, given as $V = -D[1 - \exp\{-\lambda(\Delta r - r_e)\}]^2$ when $\Delta r \geq r_e$. Here, D is the adhesion strength, Δr is the distance between the surface of the particle and cilium, r_e is the equilibrium bond length, and λ characterizes the range of interaction. The repulsive exclusion interaction of beads, particles, and walls with each other are modeled via a similar Morse potential, when $\Delta r < r_e$.

The cilia are actuated by a periodic force applied at the cilial tip given by $\mathbf{F}^{ext}(t) = F_x^0 \cos(\omega t)\cos(\psi)\mathbf{i} + F_y^0 \sin(\omega t)\mathbf{j} + F_x^0 \cos(\omega t)\sin(\psi)\mathbf{k}$, where ω is the angular frequency of actuation and ψ is the tilt (around the *y*-axis) of the plane of the effective stroke, with respect to the x–y plane. This external forcing is introduced to capture the essential features of the biological cilium's motion; namely, the cilium undergoes a configurationally asymmetric stroke, which can be partitioned into "effective" and "recovery" parts. The cilium is almost straight during the effective stroke, such that its tip sweeps a roughly circular, 180° arc, while the cilium filament is curved during the recovery stroke. The particles are caught by the adhesive cilia tips during the effective stroke. Thus, we are able to mimic observed features of the motion of the suspension feeder cilia.[2,7,22−24] Within the simulations, the positions of the cilia bead and the particles are evolved via a velocity-Verlet algorithm.

Calculated Reynolds numbers for a suspension feeder cilium in water[2,7] using the cilium length (L) and the tip velocity (ωL) yield $Re \sim 0.03^2$ and $Re \sim 0.15$,[7] indicating negligible inertial forces at the cilium length scale. We use $Re = \omega L^2/\nu = 0.1$ in our simulations (ν being the kinematic viscosity of the fluid) with the time period of the actuation $T = 2\pi/\omega = 30\,000$ LB time units. We set the other variables to the following values: $L_x/L = L_z/L = 8$, $L_y/L = 3.33$, $\lambda L = 189$, $r_e/L = 0.055$, and $a/L = 0.0167$, where a is the radius of the cilium. Given that $I = \pi a^4/4$ is the area moment of inertia of the cilium and E_0 is the reference case Young's modulus, the sperm number[10] for our system is given by $\mathrm{Sp}(E_0) = L[4\pi\eta\omega/E_0 I]^{1/4} = 4.45$. Additionally, we set $F_x^0 L^2/EI = 60$ and $F_y^0/F_x^0 = 1/2$. Simulations were performed with cilia stiffness $E = 3E_0$, for a range of adhesion strengths $0.5D_0 \leq D \leq 3D_0$ with $D_0 = F_x^0/2\lambda$. Four independent simulations were carried out for each adhesion for 60 actuation cycles.

RESULTS AND DISCUSSION

Sample trajectories of a large ($R_L = 6$ LB unit) and a small ($R_S = 3$ LB unit) particle from a mixture of particles ($\phi = 0.33$, $f = 0.53$) are shown in Figure 1b for a particular adhesion strength ($D/D_0 = 1.5$). Both large and small particles undergo net motion in the *x*-direction due to a combination of fluid advection and pushing/pulling by the cilia.[10] Notably, the particle motion in the *y* direction differs significantly based on particle size. Small particles are captured by the cilia and stay at a low average height in the cilia layer, with periodic variation in their *y* positions. Large particles, however, are pushed away from the layer, showing little fluctuations in their *y* positions. This plot indicates that the adhesive cilia can selectively capture small particles from the mixture and act as a size-based particle separator.

The total concentration of the particles, ϕ, and composition of the mixture, f, is measured in terms of the projected area of

dx.doi.org/10.1021/la400318f | Langmuir XXXX, XXX, XXX–XXX

the particles. For a mixture of particles with N_L large particles and N_S small particles, $\phi = \pi(N_L R_L^2 + N_S R_S^2)/L_x L_z$ and $f = N_L R_L^2/(N_L R_L^2 + N_S R_S^2)$. Figure 2a shows the fraction of small

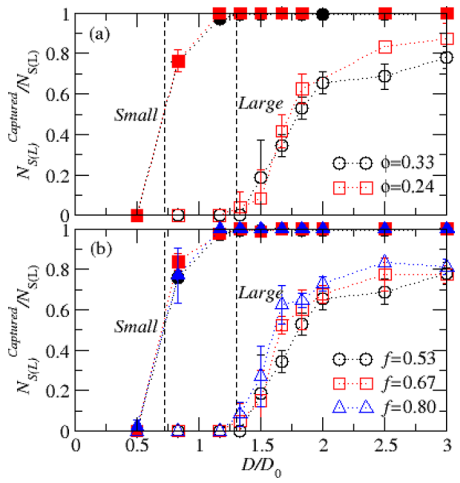

Figure 2. Number fraction of small (filled symbols) and large (open symbols) particles captured for different adhesion strengths for (a) different total concentrations of the particles with $f \approx 0.54$ and (b) different compositions of mixture for $\phi = 0.33$. Dashed vertical lines indicate the critical adhesion values for isolated small and large particles.

and large particles captured for two different total concentrations $\phi = 0.33$ ($N_S = 28$, $N_L = 8$, $f = 0.53$) and $\phi = 0.24$ ($N_S = 20$, $N_L = 6$, $f = 0.55$), which encompass almost the same compositions of the large and small particles. The particles are considered as "captured" if they are pulled bellow the adhesive part of the cilia layer, i.e., $\langle \tilde{r}_y^s \rangle < 0.66L + R$. Figure 2b shows the fraction captured for three different compositions of the mixture for a total particle concentration $\phi = 0.33$. The symbols mark the data obtained from averaging over four independent simulations; the dotted lines serve as a guide to the eye.

For all the cases, none of the particles are captured for very low adhesion strengths (see Figure 2). Increasing the adhesion leads to the capture of small particles. In effect, a nearly complete separation of the particles is achieved for a range of adhesion strengths, where small particles are selectively captured by the cilia. To gain insight into this behavior, we also examined systems containing a single, isolated particle and calculated the critical adhesion strength required to capture this particle for two different particle sizes. The critical adhesion values from these isolated particle studies are shown by the dashed vertical lines in Figure 2. The range of adhesion strengths yielding size selectively is evidently related to this difference in the critical adhesion strengths required to capture the single large and the small particles. Note that here we fixed the cilia stiffness at $E = 3E_0$; as shown later (see Figure 5), the critical adhesion strength required to capture the isolated large particle is found to be higher than that to capture the isolated small particle for any given stiffness of the cilia.

A further increase in adhesion causes the large particles to also be captured by the cilia. A greater number of large particles are captured with increasing adhesion, making the cilia less selective at higher adhesion strengths. At the lower adhesion, however, we clearly observe the preferential capture of small particles from a mixture of particles by the adhesive cilia. We emphasize that the size separation effect is observed for different compositions of the mixture and different total concentrations of the particles, including the mixture that involves an equal number of large and small particles (Figure 2b, $f = 0.8$; $N_S = N_L = 12$), indicating that the results are quite robust.

We note that the particle concentrations considered here correspond to moderately concentrated systems. For very low particle concentrations, the effect introduced by other particles would be negligible and the system would be equivalent to the case of isolated particles.[10] For such dilute systems, the variation of captured fraction with adhesion strength would resemble a step change at the critical adhesion (shown as the dotted line in Figure 2), as opposed to the gradual variation observed in Figure 2. The upper limit of the particle concentrations in our study is constrained by the fact that we maintain a 2 LB unit gap between the particle surfaces to accurately capture the hydrodynamic interaction between the particles, allowing us to explore values of $\phi < 0.42$.

We explain this preferential capture of the small particles over large ones by adapting an analytical model[10] that was used to predict the adhesion strength above which dilute monodisperse particles are captured by the adhesive cilia.[25] Here, we account for the size dependence of the particle mobility near flat walls; as we show below, this effect plays a critical role in the observed size-based particle separation.

The analytical model[10] describes the 2D motion of cilia during the effective stroke, uses lumped mass equations for cilia tip motion and couples this tip motion with the particle motion through models of bond formation and breakage between the cilia tips and particle. The position of the cilia tip is given by local coordinates $\mathbf{r}(t) = X(t)\mathbf{i} + Y(t)\mathbf{j} = r(t)\hat{\mathbf{r}}$ ($\mathbf{r} = 0$ being the tether point of the cilium) and is evolved for the effective stroke by equating the elastic and external forces and moments on the cilium with the viscous drag

$$\dot{\mathbf{r}} = \dot{r}\hat{\mathbf{r}} + r\dot{\theta}\hat{\boldsymbol{\theta}} = \boldsymbol{\mu}^{-1}[-\nabla_r U^E(\mathbf{r}) + \mathbf{F}^{ext}(t)]. \quad (1)$$

Here, $\mathbf{F}^{ext}(t)$ is the external periodic force applied on the tip and the elastic forces are obtained from the elastic energy of the cilium $U^E = {}^1/_2[k_r(r - L)^2 + k_\theta(\pi/2 - \theta)^2]$, with k_r and k_θ being the respective stretching and bending modulus. The mobility matrix of the cilia, $\boldsymbol{\mu}^{-1}$, obtained using the approximations of the resistive force theory for a rigid cylindrical rod,[26] is defined as $\mu_{r\theta}^{-1} = \mu_{\theta r}^{-1} = 0$, $\mu_{rr}^{-1} = 2/(\alpha 2\pi\eta L/\ln(L/a))$, $\mu_{\theta\theta}^{-1} = 3/(\alpha 4\pi\eta L/\ln(L/a))$, and α accounts for the increase in mobility due to the cooperative hydrodynamic interactions of the closely spaced neighboring cilia. Values of k_r, k_θ, and α are calibrated from simulations.[10] The average local position vector of the cilia tips attached to the particle (denoted as $\bar{\mathbf{r}}(t)$) lag behind the free cilia tips (local position vector $\mathbf{r}(t)$, see Figure 3) and is evolved as

$$\frac{d\bar{\mathbf{r}}}{dt} = \frac{2(\mathbf{r} - \bar{\mathbf{r}})}{d}\dot{d} + \boldsymbol{\mu}^{-1}[-\nabla_{\bar{\mathbf{r}}} U^E(\bar{\mathbf{r}}) + \mathbf{F}^{ext}(t) + \mathbf{F}^{Morse}(r_y^s, \bar{r}_y)] \quad (2)$$

accounting for the adhesive Morse potential force $\mathbf{F}^{Morse}(r_y^s, \bar{r}_y) = -\partial V(|r_y^s - R - \bar{r}_y|)/\partial \bar{r}_y \mathbf{j}$ (identical to the LBM simulation) acting on the attached cilia due to the bond formation with the particle. The radius of the spherical cap over which the bonds are formed, d, is given in terms of the depth of the sphere in the cilia layer $\delta = Y - r_y^s - R'$, i.e., $d = (2R'\delta)^{1/2}$ and is evolved using

dx.doi.org/10.1021/la400318f | Langmuir XXXX, XXX, XXX–XXX

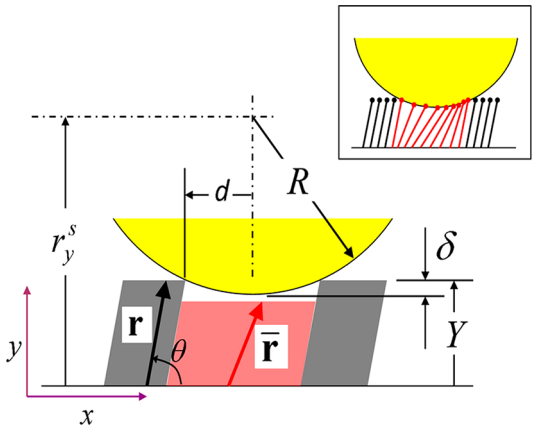

Figure 3. Schematic of cilia−particle interaction used in the analytical model.

$$\dot{d} = \frac{R'(\dot{Y} - \dot{r}_y^s)}{2d} \quad \text{for all } \delta > 0 \text{ and } (\dot{Y} - \dot{r}_y^s) \geq 0 \tag{3}$$

assuming that the bonds are formed only when the cilia approach the particle and number of bonds do not change ($\dot{d} = 0$) when the cilia recedes away from the particle ($\dot{Y} - \dot{r}_y^s < 0$). Here $R' = R + r_e + r_c$ is the relevant radius of interaction.[27] The number of bonds formed between the particle and cilia layer over the spherical cap of radius d is $n = \rho_c \pi d^2$ where $\rho_c = 1/\delta_x^2$ is the grafting density of the cilia. The equation of motion of the spherical particle, due to the pull and push from n bonds, is written from the balance of the adhesion and hydrodynamic drag forces

$$\dot{r}_y^s = \frac{-nF_y^{\text{Morse}}(r_y^s, \bar{r}_y)}{\beta 6\pi\eta R} \tag{4}$$

where the factor β accounts for the correction to the Stokes drag due to the presence of confining walls. Variables $\mathbf{r}$, $\bar{\mathbf{r}}$, d, and r_y^s are evolved using eqs 1−4 over $0 \leq t \leq T/2$ (effective stroke) with initial conditions at $t = 0$: $\mathbf{r}(0) = \bar{\mathbf{r}}(0) = L \cos\theta_0\, \mathbf{i} + L \sin\theta_0 \mathbf{j}$, $d = 0$, $\mathbf{r}_y^s(0) = R + 0.77L$, with $\theta_0 \approx 0.22$ rad. We seek a periodic particle trajectory $\tilde{r}_y^s(t)$ with the same time period as that of effective stroke, i.e., $\tilde{r}_y^s(T/2) = \tilde{r}_y^s(0)$, and the solution is obtained iteratively over several cycles of the effective stroke, assigning the $r_y^s(0)$ for a cycle to $r_y^s(T/2)$ from the previous cycle until $|\tilde{r}_y^s(T/2) - \tilde{r}_y^s(0)|$ (for the same iteration) converges to zero. Using this approach, we obtain the height variance h' of the particle for a range of adhesion and stiffness. The particle is considered to be "captured" if the scaled height variance $h'/L > \varepsilon = 5 \times 10^{-3}$.

The factor β in eq 4 characterizes the effect of the channel walls on the drag force that acts on the particle. This drag force resists the particle motion in the direction normal to the wall. From previous studies,[28,29] we anticipate that β should depend on particle size relative to it is distance from the channel walls. This factor is estimated for different particle sizes, using separate LBM simulations, as follows. A spherical particle of radius R, placed at a distance y from a flat wall, is pushed toward this wall by a constant force F_y in the negative y-direction (see inset in Figure 4a) over a distance of 3−4 LB units and the velocity of the particle v_y is obtained. To accurately estimate the factor β, the distance of the particle from the flat wall is $y \approx L + R$, i.e., approximately at the same position as in the case of the ciliated surface. Figure 4a shows the variation of the applied

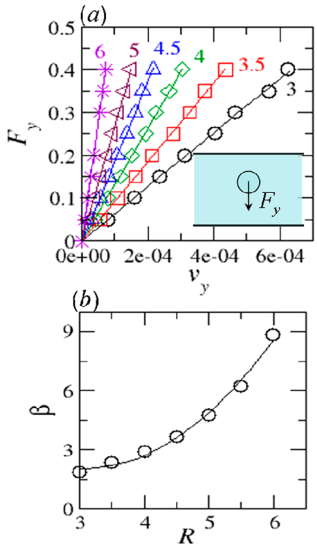

Figure 4. (a) Applied force F_y varies linearly with particle velocity v_y for different size (reported next to fitted line) particles confined between walls. Inset shows schematic of the LBM setup used for estimating factor β. (b) Variation of factor β with particle radius R (in LB units). Symbols are simualtion results and lines are fit to the data.

force F_y with the velocity v_y for different radii (reported next to the fitted line) of the particles. Symbols are simulation results and the lines are a fit to the data. As expected for low Reynolds number, we find a linear variation of F_y with v_y. The factor β is obtained as the ratio of the slope of the fitted line to $6\pi\eta R$ and shows a quadratic variation with particle size R (solid line in Figure 4b). These values of β match well with the theoretical values for the correction to the Stokes drag obtained by linearly superimposing the contribution from each flat wall.[30,31] We use the fitted values of β from Figure 4b in our analytical model to obtain the critical adhesion (above which the particles are captured by the cilia). As explained below, according to the analytical model, the size dependence in β is critical toward obtaining size selectivity of the adhesive cilia.

Since the analytical model ignores hydrodynamic interactions between particles, we performed LBM simulations for an isolated particle, for two different radii to validate the analytical model. Different stiffness $E_0 \leq E \leq 6E_0$ and adhesion strengths $0.5D_0 \leq D \leq 4D_0$ were considered and four runs for each (E, D) were performed. The external force applied at the tip was scaled with the cilia stiffness to create similar cilial motion for different stiffness[10] and the ratio $F_y^0/F_x^0 = 1/2$ was fixed. The critical adhesion obtained via the LBM simulations (using the height variance criteria) for the two sizes is shown by symbols in Figure 5. Solid lines in Figure 5 are the analytical model predictions, which compare well with the simulation results, especially for the higher cilia stiffness. The deviations from the simulation results for low cilia stiffness is expected since the assumption that the cilia can be modeled as a straight rod during the effective stroke is valid only for stiff cilia. Both the analytical model and simulations reveal that the critical adhesion above which the large particles ($R = 6$) are captured by the cilia is higher than that for the small particle ($R = 3$). Thus, we conclude that (a) hydrodynamic interactions between the particles play a secondary role in the particle-separation effect and (b) the analytical model predicts the existence of a range of adhesion strengths for which this particle-separation effect is operative.

dx.doi.org/10.1021/la400318f | Langmuir XXXX, XXX, XXX−XXX

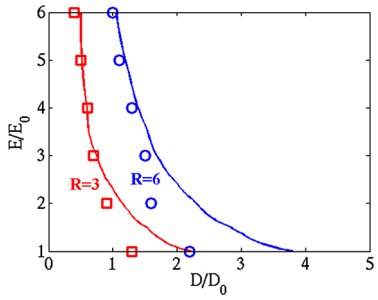

Figure 5. Critical adhesion strength (D) with cilia stiffness (E) for two different particle sizes. Symbols are simulation results, and lines are predictions from the model.

To further explain the particle separation mechanism, we note that eq 4 states that the adhesion force on the particle due to the n bonds formed with the cilia layer is balanced by the hydrodynamic drag force on the particle. When β is independent of R, the higher viscous drag for a larger particle is balanced by the higher number of bonds formed due to the larger contact area with the cilia surface, since $n \propto d^2 \propto R'\delta$. Due to the presence of channel walls (i.e., when β increases with R), however, the compensation from the larger number of bonds n is not sufficient to overcome the increased viscous drag for the larger particle, and hence, a higher adhesion is needed to capture the larger particles. Neglecting the dependence of β on particle size, therefore, fails to predict the higher adhesion strengths needed to capture the large particles. In other words, as the adhesive cilia bring the particles close to the substrate, the wall−particle hydrodynamic interactions play a critical role in the observed effect. Since the selective capture of the small particles arises from the competition between the drag and adhesion forces, and the drag force increases with size (Figure 4), increasing (decreasing) the size difference between the particles will increase (decrease) the difference between the critical adhesion strengths, allowing a large (small) range of adhesion strengths for the selective capture of the small particles for any particular stiffness of the cilia.

CONCLUSIONS

Using adhesive artificial cilia, we could mimic the size selective behavior displayed by suspension feeders. We demonstrated that the size separation can arise simply due to the competition of adhesive and hydrodynamic forces. The drag on the larger particles increases substantially in the channel, and for a given cilia adhesive strength, there exists a particle size beyond which the adhesion force is insufficient to capture the particles. As indicated in Figure 1b, the motile, adhesive cilia not only capture the particles but also move the particles along the surface. Our findings suggest that actuated artificial cilia with adhesive tips can be used as an effective means of separating different sized particles in microfluidic devices even at low Reynolds numbers (Re) by appropriately tuning the adhesion strength and the cilia stiffness. We note that size separation mechanisms utilizing inertial migration of the particles[32−34] cannot be used at $Re < 1$, where inertial forces become negligible.

With the increasing interest in using actuated cilia arrays as microfluidic pumping/mixing devices, our findings reveal the additional potential of actuated adhesive ciliated arrays for selectively transporting microscopic particles based on their size. More specifically, an important application for microfluidic devices is the sorting or trapping of biological cells.[35] Hence, establishing effective means of sorting particles within fluid-filled microchannels is key to advances in biomedical assays. Our results indicate that adhesive, actuated artificial cilia can play a vital role in such devices, promoting the separation of cells by size. Notably, separation of particular cells that differ in size is essential for cellular therapies, and pharmacological and metabolic studies.[18]

In the above simulations, we related the critical adhesion strengths for capturing the different sized particles to parameters that characterize the cilium and the surrounding fluid. Below, we use the values of parameters for a biological cilium in water to show that the predicted adhesion strengths are comparable to actual cell adhesion energies reported in the literature. Hence, the relevant values used in the model are physically realistic and physically realizable. With these values as guidelines, the behavior could potentially be replicated in synthetic ciliated surfaces as well as being observed in scenarios involving biological species.

Using the typical values that characterize biological cilium, we specify the length of the cilium to be $L = 60\ \mu$m and beating frequency to $1/T = 15$ Hz.[7,22,36] Assuming water as the surrounding fluid (density $\rho = 10^3$ kg/m^3 and kinematic viscosity $\nu = \eta/\rho = 10^{-6}$ m^2/s), the parameters used in the simulations ($a/L = 0.0167$, $L[4\pi\eta\omega/E_0I]^{1/4} = 4.45$, $E/E_0 = 3$, $\lambda L = 189$, $R_S/L = 1/3$, and $R_L/R_S = 2$) suggest that the radius of the cilium is $a = 1\ \mu$m (similar to reported values[36]), the inverse of the length scale over which the Morse potential decays is $\lambda = 3.15 \times 10^6$ m^{-1}, the area moment of inertia of the cilium is 7.85×10^{-25} m^4, and the Young's modulus of the cilium is $E = 0.149$ MPa. The flexural rigidity of the cilium (EI) obtained from these values is 1.17×10^{-10} dyn·cm^2. The latter value is in good agreement with the experimental values of $(2-3) \times 10^{-10}$ dyn·cm^2 reported using direct measurement of the forces and curvature of a biological cilium.[36]

Using these values, along with other parameters used in the simulations ($D_0 = F_x^0/2\lambda$, $F_x^0 = 60EI/L^2$), we can specify the adhesion energy $\gamma = D/\pi a^2$ and adhesion strength $\sigma = D\lambda/2\pi a^2$ of the cilia tips per unit area required for selective capture of small particles. For a mixture of $R_S = 20\ \mu$m and $R_L = 40\ \mu$m particles, the minimum adhesion energy required for capturing smaller particles is $\gamma = 69.3\ \mu$J/m^2 (corresponding to $D = 0.7D_0$) with adhesion strength $\sigma = 109.15$ Pa, whereas for capturing the large particles, the adhesion energy is $\gamma = 128.7\ \mu$J/m^2 (corresponding to $D = 1.3D_0$) with adhesion strength $\sigma = 202.70$ Pa. These values of the adhesion energy compare well with the estimated values of adhesion energy of motile cells[37] (~20 μJ/m^2) and model-cell microcapsules[38,39] (~0.05 mJ/m^2; ~0.026 mJ/m^2) adhering to surfaces. Mucus adhesion has been postulated to be the reason for cilia adhesion,[7] and our calculated values of the adhesion strength compare well with the maximum adhesive stress reported for mucoadhesives[40] (~1 kPa).

AUTHOR INFORMATION

Corresponding Author

*E-mail: balazs@pitt.edu.

Notes

The authors declare no competing financial interest.

dx.doi.org/10.1021/la400318f | *Langmuir* XXXX, XXX, XXX−XXX

■ ACKNOWLEDGMENTS

The authors gratefully acknowledge financial support from ONR.

■ REFERENCES

(1) den Toonder, J. M.; Onck, P. R. Microfluidic Manipulation with Artificial/Bioinspired Cilia. *Trends Biotechnol.* **2013**, *31* (2), 85−91.
(2) Strathmann, R. R.; Jahn, T. L.; Fonseca, J. Suspension Feeding by Marine Invertebrate Larvae: Clearance of Particles by Ciliated Bands of a Rotifer, Pluteus, and Trochophore. *Biol. Bull.* **1972**, *142*, 505−519.
(3) LaBarbera, M. Water Flow Patterns in and around Three Species of Articulate Brachiopods. *J. Exp. Mar. Biol. Ecol.* **1981**, *55*, 185−206.
(4) LaBarbera, M. Feeding Currents and Particle Capture Mechanisms in Suspension Feeding Animals. *Am. Zool.* **1984**, *24*, 71−84.
(5) Taghon, G. L. Optimal Foraging by Deposit-Feeding Invertebrates: Roles of Particle Size and Organic Coating. *Oecologia* **1982**, *52*, 295−304.
(6) Jumars, P. A.; Self, R. F. L.; Nowell, A. R. M. Mechanics of Particle Selection by Tentaculate Deposit-Feeders. *J. Exp. Mar. Biol. Ecol.* **1982**, *64*, 47−70.
(7) Romero, M. R.; Kelstrup, H. C. P.; Strathmann, R. R. Capture of Particles by Direct Interception by Cilia during Feeding of a Gastropod Veliger. *Biol. Bull.* **2010**, *218*, 145−159.
(8) Fritz, L. W.; Lutz, R. A.; Foote, M. A.; VanDover, C. L.; Ewart, J. W. Selective Feeding and Grazing Rates of Oyster (Crassostrea virginica) Larvae on Natural Phytoplankton Assemblages. *Estuaries* **1984**, *7*, 513−518.
(9) Shimeta, J.; Koehl, M. A. R. Mechanism of Particle Selection by Tentaculate Suspension Feeders during Encounter, Retention, and Handling. *J. Exp. Mar. Biol. Ecol.* **1997**, *209*, 47−73.
(10) Bhattacharya, A.; Buxton, G. A.; Usta, O. B.; Balazs, A. C. Propulsion and Trapping of Microparticles by Active Cilia Arrays. *Langmuir* **2012**, *28*, 3217−3226.
(11) Mayer, S. Modelling of Ciliary Downstream Collecting in Suspension-Feeding Invertebrates. *Math. Models Methods Appl. Sci.* **2001**, *24*, 1409−1427.
(12) Ghosh, R.; Buxton, G. A.; Usta, O. B.; Balazs, A. C.; Alexeev, A. Designing Oscillating Cilia That Capture or Release Microscopic Particles. *Langmuir* **2010**, *26*, 2963−2968.
(13) Masoud, H.; Alexeev, A. Harnessing Synthetic Cilia to Regulate Motion of Microparticles. *Soft Matter* **2011**, *7*, 8702−8708.
(14) Sleigh, M. A. Adaptations of Ciliary Systems for the Propulsion of Water and Mucus. *Comp. Biochem. Physiol.* **1989**, *94A*, 359−364.
(15) Norwood, J. T.; Hein, C. E.; Halbert, S. A.; Anderson, R. G. W. Polycationic Macromolecules Inhibit Cilia-Mediated Ovum Transport in the Rabbit Oviduct. *Proc. Natl. Acad. Sci. U. S. A.* **1978**, *75* (9), 4413−4416.
(16) Talbot, P.; Riveles, K. Smoking and Reproduction: the Oviduct As a Target of Cigarette Smoke. *Reprod. Biol. Endocrinol.* **2005**, *3*, 52.
(17) den Toonder, J.; Bos, F.; Broer, D.; Filippini, L.; Gillies, M.; deGoede, J.; Mol, T.; Reijme, M.; Talen, W.; Wilderbeek, H.; Khatavkar, V.; Anderson, P. Artificial Cilia for Active Micro-fluidic Mixing. *Lab Chip* **2008**, *8*, 533−541.
(18) Yamada, M.; Kano, K.; Tsuda, Y.; Kobayashi, J.; Yamato, M.; Seki, M.; Okano, T. Microfluidic Devices for Size-Dependent Separation of Liver Cells. *Biomed. Microdevices* **2007**, *9*, 637−645.
(19) Shevkoplyas, S. S.; Yoshida, T.; Munn, L. L.; Bitensky, M. W. Biomimetic Autoseparation of Leukocytes from Whole Blood in a Microfluidic Device. *Anal. Chem.* **2005**, *77*, 933−937.
(20) Ladd, A. J. C. Numerical Simulations of Particulate Suspensions via a Discretized Boltzmann Equation. Part 1. Theoretical Foundation. *J. Fluid. Mech.* **1994**, *271*, 285−309.
(21) Ahlrichs, P.; Dunweg, B. Lattice-Boltzmann Simulation of Polymer-Solvent Systems. *Int. J. Mod. Phys. C* **1998**, *9*, 1429−1438.
(22) Pernet, B.; Strathmann, R. R. Opposed Ciliary Bands in the Feeding Larvae of Sabellariid Annelids. *Biol. Bull.* **2011**, *220*, 186−198.
(23) Gray, J. The Mechanism of Ciliary Movement. *Proc. R. Soc. London, B* **1922**, *39*, 104−121.
(24) Carter, G. S. On the Structure and Movements of the Latero-Frontal Cilia of the Gills of *Mytilus*. *Proc. R. Soc. London, B* **1924**, *96*, 115−122.
(25) We utilize the term "captured" as used in the suspension feeder literature and emphasize that it is identical to the "propelled" state of ref 10, as the captured particles are transported along the layer.
(26) Brennen, C.; Winet, H. Fluid Mechanics of Propulsion by Cilia and Flagella. *Annu. Rev. Fluid Mech.* **1977**, *9*, 339−398.
(27) $r_c = 9(\ln 2)/\lambda$ is the bond interaction distance from the equilibrium bond length over which the Morse force decays to less than 1% of the maximum bond force.
(28) Brenner, H. The Slow Motion of a Sphere through a Viscous Fluid Towards a Plane Surface. *Chem. Eng. Sci.* **1961**, *16*, 242−251.
(29) Cox, R. G.; Brenner, H. The Slow Motion of a Sphere through a Viscous Fluid Towards a Plane Surface—II Small Gap Widths, Including Inertial Effects. *Chem. Eng. Sci.* **1967**, *22*, 1753−1777.
(30) Lin, B.; Yu, J.; Rice, S. A. Direct Measurements of Constrained Brownian Motion of an Isolated Sphere between Two Walls. *Phys. Rev. E* **2000**, *62*, 3909−3219.
(31) Happel, J.; Brenner, H. *Low Reynolds Number Hydrodynamics, Mechanics of Fluids and Transport Processes*; Kluwer: Dordrecht, 1983; Vol. *1*.
(32) DiCarlo, D.; Irimia, D.; Tompkins, R. G.; Toner, M. Continuous Inertial Focusing, Ordering and Separation of Particles in Microchannels. *Proc. Natl. Acad. Sci. U. S. A.* **2007**, *104*, 18892−18897.
(33) Bhagat, A. A. S.; Kuntaegowdanahalli, S. S.; Papautsky, I. Continuous Particle Separation in Spiral Microchannels Using Dean Flows and Differential Migration. *Lab Chip* **2008**, *8*, 1906−1914.
(34) Kuntaegowdanahalli, S. S.; Bhagat, A. A. S.; Kumar, G.; Papautsky, I. Inertial Microfluidics for Continuous Particle Separation in Spiral Microchannels. *Lab Chip* **2009**, *9*, 2973−2980.
(35) Zhu, G.; Nguyen, N.-T. Particle Sorting in Microfluidic Systems. *Micro Nanosyst.* **2010**, *2*, 202−216.
(36) Baba, S. A. Flexural Rigidity and Elastic Constant of Cilia. *J. Exp. Biol.* **1972**, *56*, 459−467.
(37) Simson, R.; Wallraff, E.; Faix, J.; Niewohner, J.; Gerisch, G.; Sackmann, E. Membrane Bending Modulus and Adhesion Energy of Wild-Type and Mutant Cells of Dictyostelium Lacking Talin or Cortexillins. *Biophys. J.* **1998**, *74*, 514−522.
(38) Liu, K. K.; Chan, V.; Zhang, Z. Capsule-Substrate Contact Deformation: Determination of Adhesion Energy. *Med. Biol. Eng. Comput.* **2002**, *40*, 491−495.
(39) Elsner, N.; Dubreuil, F.; Fery, A. Tuning of Microcapsule Adhesion by Varying the Capsule-Wall Thickness. *Phys. Rev. E* **2004**, *69*, 031802.
(40) Merkle, H. P.; Anders, R.; Wermerskirchen, A. Mucoadhesive buccal patches for peptide delivery. In *Bioadhesive Drug Delivery Systems*; Lenaerts, V., Gurny, R., Eds.; CRC Press: Boca Raton, FL, 1990; pp 105−136.